A CCD IMAGE TRANSDUCER AND PROCESSOR SUITABLE FOR SPACE FLIGHT

Donald J. Michels

E. O. Hulburt Center for Space Research
Naval Research Laboratory
Washington, D. C.

A satellite-borne extreme-ultraviolet solar telescope under development at the Naval Research Laboratory makes use of CCD area arrays for both image readout and on-board data processing. The instrument is designed to view the inner solar corona in the wavelength band 170 - 630 Å, and the output video stream may be selected by ground command to present the coronal scene, or the time-rate-of-change of the scene.

Details of the CCD application to on-board image processing will be described, and a discussion of the processor's potential for telemetry bandwidth compression is included. Optical coupling methods, data storage requirements, spatial and temporal resolution, and nonsymmetry of resolution (pitch) in the CCD will be discussed. Laboratory simulations of system performance using solar data from previous space flights will be presented.

I. REQUIREMENTS OF SPACE IMAGING SYSTEMS

Increasing availability of stabilized, accurately pointed space platforms has accelerated development of sophisticated imaging systems designed to be used in a space environment and operated in automatic or remotely controlled mode. Requirements for space telescopes differ, in some respects, from those for ground-based imagers; therefore it is appropriate to comment briefly on system requirements before describing the telescope under development at NRL.

The components of a generalized space imaging system may be divided into three functional groups, viz.: the optical, the detection, and the processing subsystems. In Figure 1, the optical subsystem includes the first three blocks of the functional block diagram. Information, in the form of photons from a distant source, enters the system at the extreme left. The optics perform two vital functions, namely, collection of the light and formation of a real image at the focal plane. Diffraction limited optics are not yet common; thus the necessity for collecting suitable numbers of photons implies that collection efficiency is frequently the driving parameter in sizing the optics.

Because natural media do not generally intervene to limit the spectral range of radiation arriving at a space platform, and because radiations in widely different parts of the spectrum usually arise from distinct physical mechanisms, some method of passband limitation is almost always employed. This is indicated by the second block in Figure 1b. In some cases (third block), there may follow a stage of image intensification and/or conversion to visible wavelengths. It is possible to introduce considerable flexibility at this stage: for example, an amplified image containing a very broad range of irradiance values may be compressed by nonlinearity in the intensifier gain or the output phosphor. If this can be accomplished without blooming or other deleterious consequences, the effect may be to reduce demands on the detector.

In the detector subsystem, information is converted from the domain of quantum mechanical photons, or electron clouds, to macroscopic, or analog, electrical signals. Additionally, because the bandwidths required for parallel transmission of two-dimensional arrays are prohibitive, another necessary function of the detector subsystem is to serialize the picture

information. This reduces the data flow to a single sequential stream requiring only one telemetry channel. Both internal (self-) scanning and external (mechanical) rasters are widely used for this purpose.

In the processing subsystem are included the functions of amplification, on-board image processing (if any), digitization, formatting, buffer storage, and readout into the spacecraft telemetry system. The spacecraft system accepts data at times determined by appropriate readout gates, which it supplies, and also provides power, stabilization, timing, and other necessaries to the experiment.

The requirements for a space imaging system include sensitivities down to a few photons per picture element (pixel) per second, and dynamic range ≥ 100. Spatial resolution in excess of 10^5 pixels is frequently desired, though imagers of lower resolution also find application. In addition to total number of pixels, resolution element density is also of importance, because restrictions on telescope dimensions often limit the magnification possible. Other requirements include stability of gain and sensitivity, and the ability to put out data at a rate commensurate with spacecraft telemetry allocations. For video systems in small scientific satellites, this will almost always imply a capacity for image storage or slow-scan operation.

II. NRL EXTREME-ULTRAVIOLET VIDEO TELESCOPE

One configuration of the proposed NRL system is shown in Figure 1c. Designed to study the sun in the wavelength range 170 - 630 Å, this version is equipped with a Type II Wolter reflective lens. The first flight system, however, will use a normal incidence parabolic mirror in the off-axis Herschelian arrangement. The filter wheel carries six transmission filters consisting of unsupported thin films of evaporated metals. Passband is determined by the telescope reflectance folded into the transmittance curve for the filter selected.

Other than the optics and filter wheel, the remainder of the first, or optical section is largely empty; very careful attention must be paid to the nature and cleanliness of materials and surface finishes used within this compartment because of the extreme sensitivity of ultraviolet optical components to surface contaminants condensing from outgassed vapors. A second compartment, isolated from the first and third, contains the cooled

CCD detector. The third compartment contains that portion of the electronics that must be kept physically close to the detector. Remaining electronics may be housed in a separable electronics package.

III. DETECTION SUBSYSTEM

An enlarged view of the detector section is seen in Figure 2. At the focal plane of the telescope is placed a microchannel plate image intensifier (MCP) (Refs. 1 - 4). Output from this device is through a fiber-optic plate, sealed into the isolation bulkhead. A phosphor provides conversion to visible wavelengths after multiplication of the electron image by 10^3 or more in the MCP. The CCD is mounted on a substrate cooled by a simple heat radiator (Refs. 5 and 6). A second CCD, labeled B, is mounted on the same cooled pad. Chip B, which may actually be two or several discrete chips, is shielded from any light input. It is used for buffer storage and image processing. Optical coupling of the image from the MCP to CCD-A is achieved through a tapered fiber-optic, which will be discussed later.

IV. ON-BOARD IMAGE PROCESSING

Figure 3 presents, in conceptual form, the CCD readout and processing technique. The amplified, visible image (of the sun, in this application) is relayed to CCD-A for detection. The output register of chip A feeds the video data stream into an analog switching network that can route the signals into any of three paths. In the simplest case (path 1), the video image, after a suitable integration period, is clocked out, digitized, and sent through the spacecraft telemetry system to ground stations for analysis.

In a second mode, the two CCDs are used cooperatively as an optical comparator. At time t, chip A receives and records an optical image. On completion of image integration, the video signal is clocked out and routed (path 2) to the input register of chip B. After insertion, the image is stored in chip B, while a new image is recorded on chip A at time $t + \Delta t$. Then, using common clock pulse signals, the image of the scene at time t is gated out of chip B (path 4) simultaneously with readout of the scene at $t + \Delta t$ from chip A (path 3). The two signals are combined in a difference amplifier, whose output is an analog video image having the same dimensionality as

either of the two input images. The intensity values in this difference image will be zero for every picture point, unless the brightness of the scene at a given point has changed during the time Δt.

As a further refinement, when the two images are being simultaneously clocked into the difference amplifier, the signal from chip A (the scene at $t + \Delta t$) may be divided (path 2 and path 3) and used to replace the original image now being moved out of chip B. Continuous operation for a succession of images processed in this manner provides at the output of the comparator an analog video signal that displays the time-rate-of-change of brightness for each element in the scene viewed, with time resolution Δt, while retaining the full spatial resolution of a single image recorded by the same system.

The amplified difference signal may be utilized in a number of ways. Most simply, it may be entered into the telemetry data stream, particularly for use as real-time data during passes over ground stations (path 5). This allows reduction of the number of bits per data word (pixel) to that required to transmit changes only in the brightness in sampling intervals Δt.

The image points in the difference picture will, in general, have intensity values other than zero, the rms value being a measure of photon statistical noise, of system noise, and of imperfect matching of the two CCD chips. It will be useful therefore to include a discriminator (which may be located in either the analog or the digital portion of the circuitry). The discriminator will pass all signals whose difference value exceeds a certain threshold level (preset by ground command), while setting all other pixel values to zero. If the number of picture elements that are poorly matched between the two chips is so large as to be troublesome, a compensating filter may be required. This too may be constructed around a CCD (linear), which is ideally suited for matched transversal filtering.

After filtering and discrimination, the number of nonzero picture points remaining in each frame will be relatively small; it becomes a simple matter to store and operate on them for the purpose of automatic decision-making.

As mentioned earlier, the telescope presently under development is optimized for observations of the sun in the ultraviolet. An important problem in solar observations is the study of solar flares. The flare manifests itself

as a sudden, highly localized brightening throughout a broad spectral range; the energy release mechanism is unknown. One of the objectives of this system is to detect, locate, and predict the occurrence of solar flares. A "decision logic" package is indicated in the diagram (Figure 3), with logic circuitry sufficient to perform basic functions such as, e.g., generation of a flare-alarm signal whenever the intensity, or rate of increase of intensity, in one pixel or a group of pixels exceeds some presettable threshold. Note that by the simple expedient of counting readout-gate pulses, the x and y position of any pixel exceeding the discriminator threshold is uniquely determined (x-y counter). The flare-alarm signal sequence will contain information on location of the flaring point, and on the rate of change of the most rapidly increasing point. The more sophisticated functions required for flare prediction, such as analysis of the time-history of brightness fluctuations in certain XUV bright points, will require substantial amounts of storage and more versatile programming; automated analysis of this type would require an on-board spacecraft computer of modest capability. This central processor (CPU) is indicated in Figure 3.

Even analysis of fluctuating bright points, however, does not make exorbitant demands on the computer. Suppose, for example, that we assume a CCD matrix of 244 × 190 pixels: it desired to track the intensity variations of the ten most active pixels (in a raster of 46,360). This requires storage of 10 intensity values (8 bits each) for each sample, plus 10 x-position and 10 y-position words (8 bits each), or 30 data words for the first sample and 10 per sample afterwards, as the position designators need not be repeated; a check can be maintained so that if a given pixel becomes inactive during a certain number of sampling intervals, its history can be erased and the next most active pixel put in its place. Image integration times may be one second or several seconds, but sampling intervals may be more widely spaced. For detection of precursors that may precede the explosive phase of a solar flare by 5 to 10 minutes, 1/4-minute sampling intervals should be sufficient. Then storage of the indicated information over a time span of 10 minutes will require 420 8-bit data words. Programming should be correspondingly straightforward. The requirements reduce basically to ordering according to peak and gradient values, and comparisons with a table of ground-commandable threshold levels. After each picture readout, the appropriate comparisons will be carried out,

and a decision is made either to repeat the sequence or to actuate the flare alarm sequence.

V. DATA COMPRESSION

Another use of the discriminator and logic capability is as a powerful data compression tool. For this, the CPU is not needed. A digital comparator and buffer memory is included in the logic package, which is capable of storing perhaps 1% of the total 46K pixel values, along with their x and y coordinates. Then, as each difference-picture is processed, the 460 most significant (rate-of-change) pixels are stored. In this mode, a full picture is transmitted (path 1) at intervals, then changes only are transmitted until the next reference (full) picture is due. In this way, rapidly changing scenes can be recorded with high time resolution while using only a small fraction of the telemetry that would be required for the same information in a full transmission mode.

As a test for the concept proposed here, trial runs have been made on a laboratory computer, using broadband XUV data from the NRL instrument on OSO-7. The results of such a trial are shown in Figure 4. At the top of the figure are shown seven sequential pictures of the sun in 171 - 630 Å radiation. Spaced at 8-minute intervals, they were generated by an image dissector utilizing the mechanical raster of the OSO, with 64 horizontal scan lines of 48 data words each, for a total of 3072 8-bit words per frame. In reconstructing the data for presentation in the form shown here, this matrix has been expanded by a factor of 12, so that the resultant display of 36,864 pixels approximates the proposed matrix of 46K.

Shown in the lower row of Figure 4 are difference images generated by differencing, in the computer, pairs of images from the upper row. Note that alternate, rather than successive, images are differenced. This is because the OSO was in an interlaced raster mode at the time; successive rasters were displaced from each other by a small amount. Therefore, the time interval Δt covered by each of the lower pictures is 16 minutes. While this sampling interval is longer than would be desirable for some applications, the principle is clearly illustrated. Ground observatories detected a flare of importance -N on the west limb, beginning at 1342 UT. The flare is seen as a single bright spot in the third difference frame (1344 - 1328) and, in its later phase, in the

fourth frame (1353 - 1336). An apparent precursor brightening is seen in the first difference frame (1328 - 1312). The sensitivity of the method is made more apparent if one considers the difficulty of detecting the flare by inspection of the upper images, or by such methods as looking for a change in the integrated light from the entire solar image.

Examination of the first three difference images of Figure 4 should convince one that transmission of the most variable 1% of the total number of pixels will serve a useful purpose in tracking the progress of transient phenomena, particularly when the sampling interval is short. The fourth difference frame shows, in addition to the flare, a displacement of the entire solar disc. This is because the last picture in the upper row (1353 UT) was completed just before entering the earth's shadow. Atmospheric attenuation and scattering were sufficient to cause a slight shift in the spacecraft pointing error signals. This effect may have been sufficient also to alter slightly the appearance of the flaring region in the last difference image.

VI. OPTICAL COUPLING

Figure 5 illustrates the proposed method for coupling the MCP output into CCD-A. While a relay lens could be used, there are a number of advantages to the tapered fiber-optic. Among these are (1) compactness, (2) lower transmission losses, (3) inherent ruggedness and low weight, and (4) the ability to introduce image distortions that are desirable in order that the resolution capability of the CCD may be fully realized. The dimensions of a Fairchild 244 × 190 CCD are indicated in the upper portion of the figure (5a) (Ref. 7). Neither the linear dimensions nor the spacing (pitch) of sensing elements are equal along the two scan directions. There are 244 TV lines parallel to the 5.7-mm dimension (pitch = 18 μm), with 190 picture elements per line parallel to the 4.4-mm direction (pitch = 30 μm). [Horizontal scan lines, in the TV video raster sense, run vertically in the illustration. The orientation shown would pertain when the instrument z-axis is aligned with the heliographic polar axis, as shown in the lower portion (5b).]

The solar image formed by the optics at the MCP measures 7.1 mm. Tapering of the fiber optic will demagnify the image so that it just fills the chip's sensitive area. For a solar angular diameter of 1920 arc seconds,

the 190-pixel scan line then fulfills the design requirement to locate a point source to within 10 arc seconds. Distortion of the fiber optic into an elliptical cross section compresses the solar image along the equatorial axis, thus making the resolution parallel to the equator equal to that parallel to the polar axis.* In addition, the field of view for equatorial regions is then expanded to 42 arc minutes, thus facilitating observation of off-limb transient events, which are far more common at low and middle heliographic latitudes. The format of the reconstructed solar image is shown in Figure 5b. It is seen that the 32 × 41 arc minute field of view allows observation of coronal emissions over the entire solar disc, and above the limb to a distance of 5 or 10 arc minutes, except near the poles.

As indicated earlier, the CCD detector is mounted on a pad for cooling to approximately 200°K. The necessity for cooling to reduce thermal dark current arises from the requirements of this application, in which integration and storage times of tens of seconds are essential. A paper to be presented later in this symposium will give the results of preliminary cooling experiments using a 100 × 100 imager.

VII. CONCLUSION

Figure 6 shows how the inner solar corona may look through the eye of a CCD camera. Data from a rocket flight was imaged to simulate the scene. The camera used a Fairchild CCD-201 chip. Present plans call for launch in 1977 of a simple CCD imaging system of 10^4-pixel, or greater, resolution. This first prototype will utilize the MCP, tapered fiber optic, and cooled CCD imager, but will probably not have on-board image processing capability. The full system, with improved resolution and on-board processing, is proposed for a later flight.

*High-resolution tapered fiber optics having controlled distortion were obtained from Galileo Electro-Optics Corp., Galileo Park, Sturbridge, Massachusetts.

REFERENCES

1. B. W. Manley, A. Guest, and R. T. Holmshaw, Proceedings of the Fourth Symposium on Photo-Electronic Image Devices, London, 1968; Advances in Electronics and Electron Physics, Vol. 28 A, Academic Press, New York, 1969, p. 471.
2. J. Adams, Electro-Optical Systems Design 1, 46 (1969).
3. G. R. Carruthers, Astrophysics and Space Science 14, 332 (1971).
4. W. R. Hunter and F. E. Harlow, Appl. Opt. 12, 968 (1973).
5. R. V. Annable, Appl. Opt. 9, 185 (1970).
6. R. V. Annable, Appl. Opt. 11, 1495 (1972).
7. M. Vicars-Harris, Fairchild Camera and Systems Div., Syosset, New York (private communication).

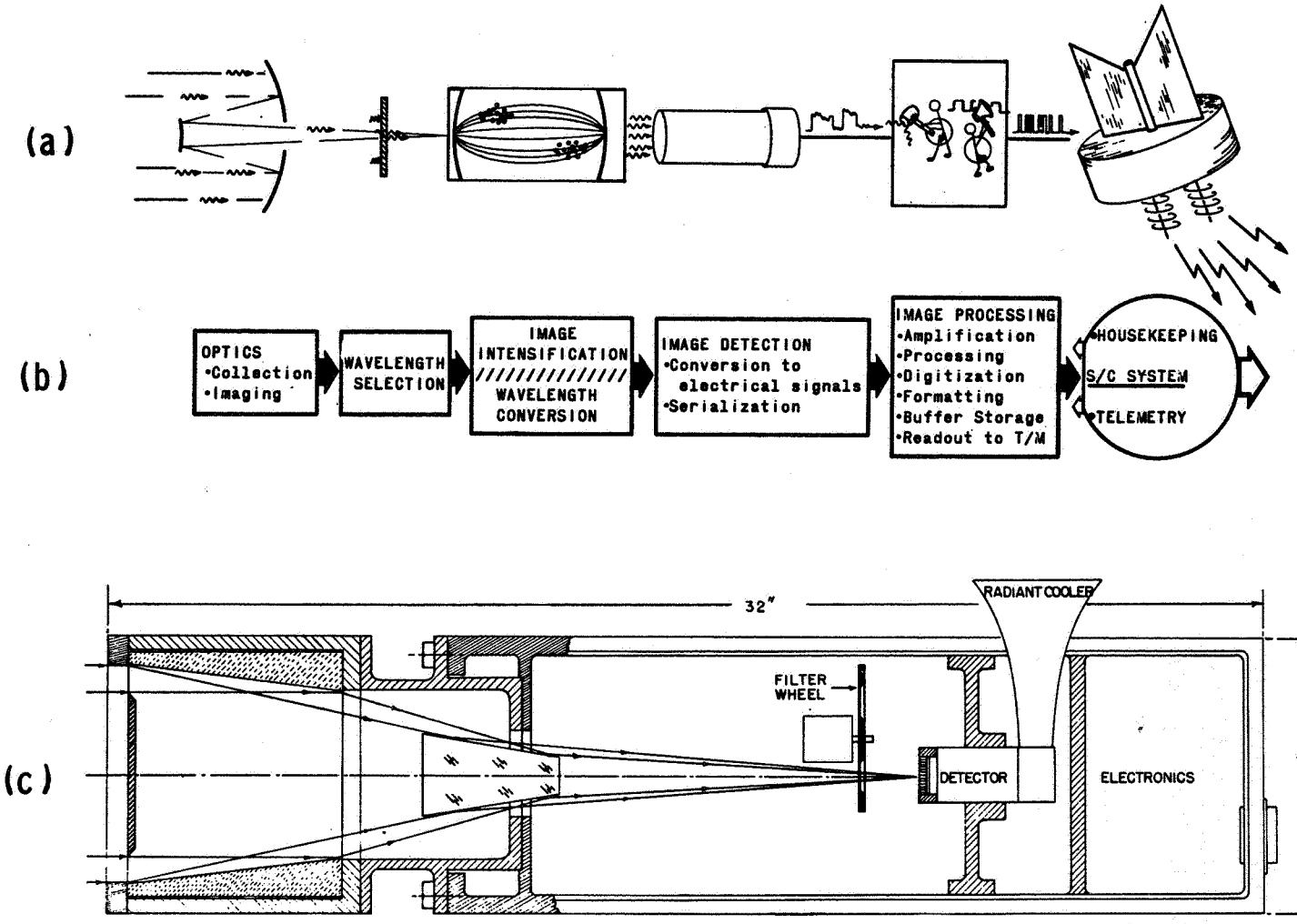

Figure 1. The various components of a generalized space imaging system in (a) diagrammatic and (b) functional block diagram form; (c) one version of the extreme-ultraviolet solar telescope under development at the Naval Research Laboratory

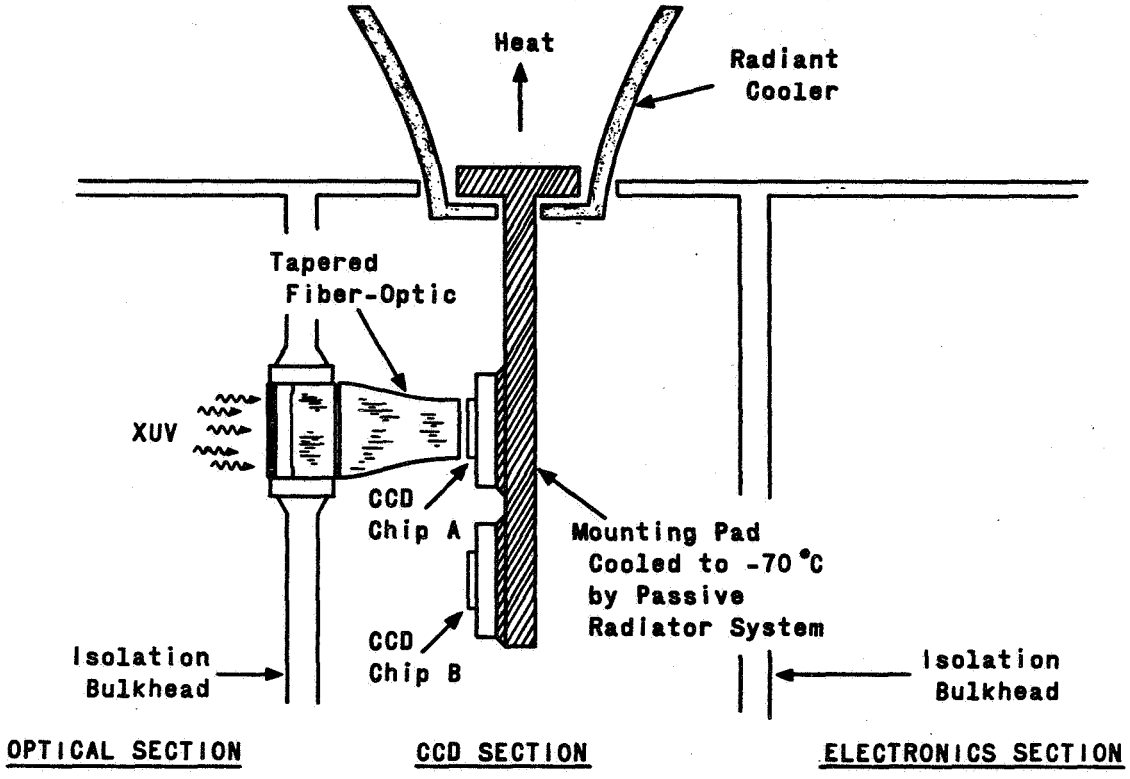

Figure 2. View of the detector section of the NRL telescope

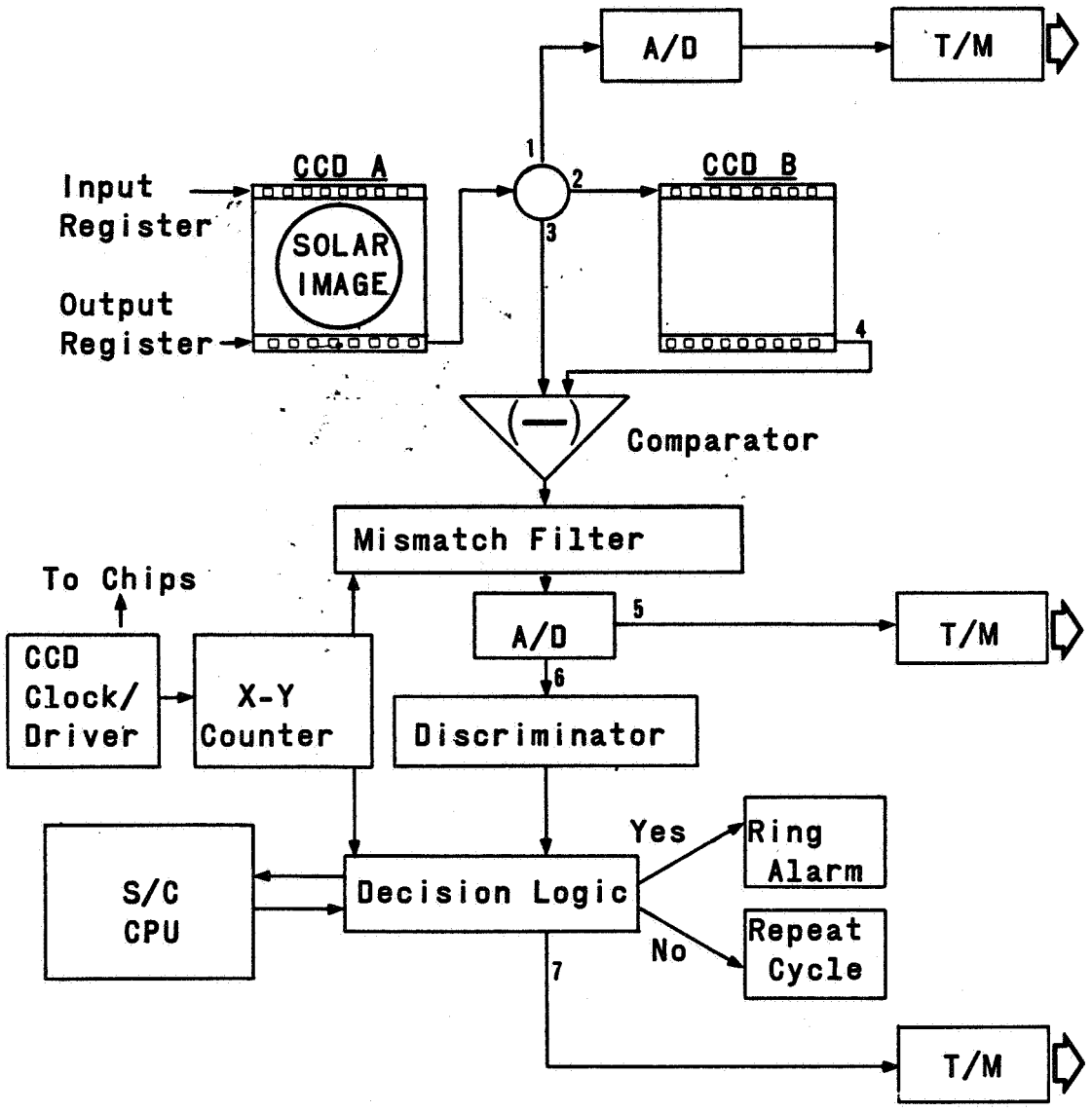

Figure 3. Functional block diagram of the CCD image transducer and processor (CCD-A is at the focal plane of the telescope; CCD-B is covered by an optical mask and receives image information only through the electrical input register.)

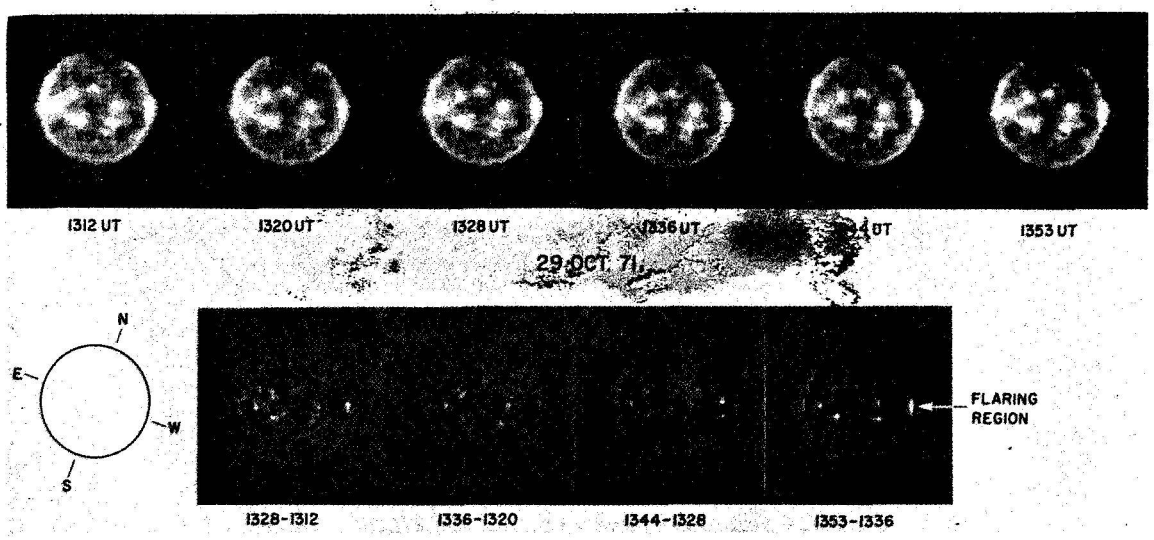

Figure 4. Laboratory simulation of optical comparator mode of operation, using solar data from the OSO-7 satellite (In the upper row are sequential 171 - 630 Å solar images; times shown are the starting times for each 8-minute raster. Below are shown differences between pairs of (alternate) images from the upper row.)

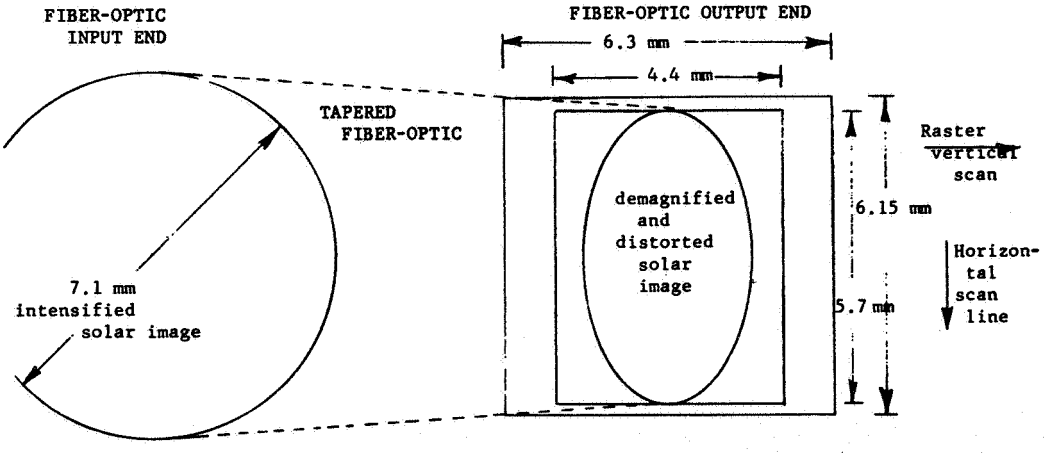

(a) FLIGHT INSTRUMENT IMAGE LAYOUT AND CHIP DIMENSIONS.

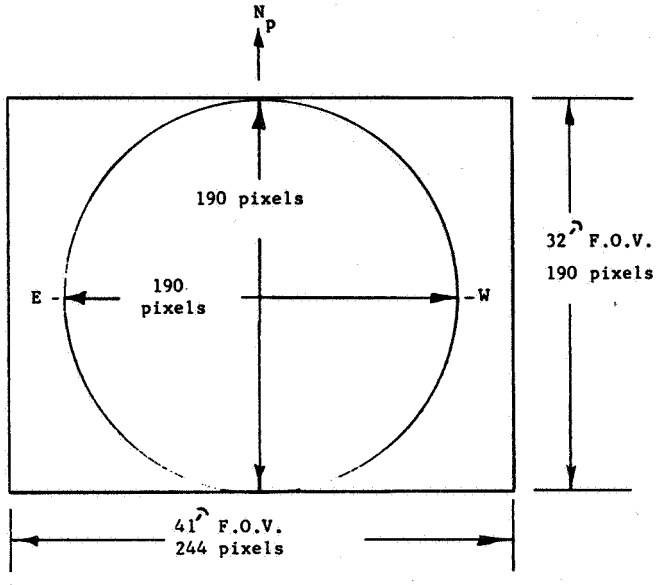

(b) RECONSTRUCTED SOLAR IMAGE.

Figure 5. Details of the optical coupling scheme, which makes use of fiber optics to both reduce and distort the image for optimum utilization of the CCD (Consult Section VI of the text for explanation.)

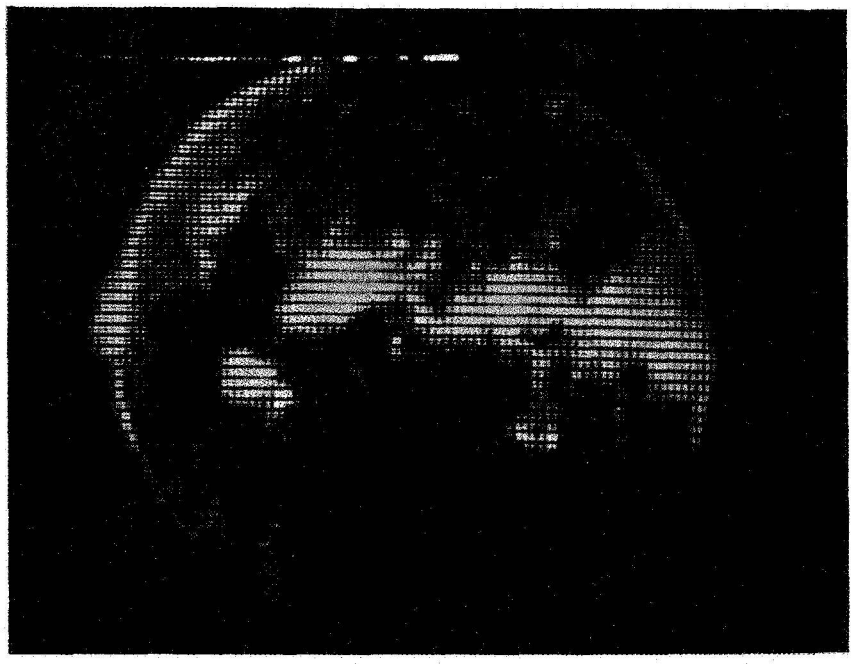

Figure 6. Laboratory simulation of solar telescope output